Double-helix enhanced axial localization in STED nanoscopy

G. P. J. Laporte,[1,*] D. B. Conkey,[2] A. Vasdekis,[3] R. Piestun,[2] and D. Psaltis[1]

[1]*Laboratory of Optics, School of Engineering, École Polytechnique Fédérale de Lausanne (EPFL), Station 17, 1015 Lausanne, Switzerland*

[2]*Department of Electrical, Computer, and Energy Engineering, University of Colorado, Boulder, Colorado 80309, USA*

[3]*Environmental Molecular Sciences Laboratory, Pacific Northwest National Laboratories, Richland, Washington 99352, USA*

[*]*gregoire.laporte@epfl.ch*

Abstract: Stimulated Emission Depletion (STED) microscopy enables subdiffraction resolution in the imaging plane. However, STED's lateral improvement in resolution is generally better than the enhancement in the axial direction. Here, we combine conventional STED superresolution imaging with Double Helix Point Spread Function (PSF) modulation for axial localization with a precision better than the classical Rayleigh limit. To demonstrate the capability of the method we resolve in a STED microscope sub-diffraction fluorescent bead assemblies, and localize them axially with better than 25nm precision. We also show that the same setup allows straightforward implementation of wide field phase contrast by imaging larger beads with spiral and dark field phase filtering.

OCIS codes: (170.2520) Fluorescence microscopy; (100.6640) Superresolution; (170.6900) Three-dimensional microscopy.

References and links

1. E. Betzig, G. H. Patterson, R. Sougrat, O. W. Lindwasser, S. Olenych, J. S. Bonifacino, M. W. Davidson, J. Lippincott-Schwartz, and H. F. Hess, "Imaging intracellular fluorescent proteins at nanometer resolution," Science **313**(5793), 1642–1645 (2006).
2. S. T. Hess, T. P. Girirajan, and M. D. Mason, "Ultra-high resolution imaging by fluorescence photoactivation localization microscopy," Biophys. J. **91**(11), 4258–4272 (2006).
3. S. R. P. Pavani and R. Piestun, "Three dimensional tracking of fluorescent microparticles using a photon-limited double-helix response system," Opt. Express **16**(26), 22048–22057 (2008).
4. S. R. P. Pavani, M. A. Thompson, J. S. Biteen, S. J. Lord, N. Liu, R. J. Twieg, R. Piestun, and W. E. Moerner, "Three-dimensional, single-molecule fluorescence imaging beyond the diffraction limit by using a double-helix point spread function," Proc. Natl. Acad. Sci. U. S. A. **106**(9), 2995–2999 (2009).
5. T. A. Klar and S. W. Hell, "Subdiffraction resolution in far-field fluorescence microscopy," Opt. Lett. **24**(14), 954–956 (1999).
6. G. Donnert, J. Keller, R. Medda, M. A. Andrei, S. O. Rizzoli, R. Lührmann, R. Jahn, C. Eggeling, and S. W. Hell, "Macromolecular-scale resolution in biological fluorescence microscopy," Proc. Natl. Acad. Sci. U. S. A. **103**(31), 11440–11445 (2006).
7. G. Donnert, J. Keller, C. A. Wurm, S. O. Rizzoli, V. Westphal, A. Schönle, R. Jahn, S. Jakobs, C. Eggeling, and S. W. Hell, "Two-color far-field fluorescence nanoscopy," Biophys. J. **92**(8), L67–L69 (2007).
8. K. Y. Han, K. I. Willig, E. Rittweger, F. Jelezko, C. Eggeling, and S. W. Hell, "Three-dimensional stimulated emission depletion microscopy of nitrogen-vacancy centers in diamond using continuous-wave light," Nano Lett. **9**(9), 3323–3329 (2009).
9. T. J. Gould, D. Burke, J. Bewersdorf, and M. J. Booth, "Adaptive optics enables 3D STED microscopy in aberrating specimens," Opt. Express **20**(19), 20998–21009 (2012).
10. B. Harke, C. K. Ullal, J. Keller, and S. W. Hell, "Three-dimensional nanoscopy of colloidal crystals," Nano Lett. **8**(5), 1309–1313 (2008).
11. D. Wildanger, R. Medda, L. Kastrup, and S. W. Hell, "A compact STED microscope providing 3D nanoscale resolution," J. Microsc. **236**(1), 35–43 (2009).
12. R. Schmidt, C. A. Wurm, S. Jakobs, J. Engelhardt, A. Egner, and S. W. Hell, "Spherical nanosized focal spot unravels the interior of cells," Nat. Methods **5**(6), 539–544 (2008).

#198934 - $15.00 USD Received 7 Oct 2013; revised 17 Nov 2013; accepted 22 Nov 2013; published 9 Dec 2013

13. T. J. Gould, J. R. Myers, and J. Bewersdorf, "Total internal reflection STED microscopy," Opt. Express **19**(14), 13351–13357 (2011).
14. B. Huang, W. Wang, M. Bates, and X. Zhuang, "Three-dimensional super-resolution imaging by stochastic optical reconstruction microscopy," Science **319**(5864), 810–813 (2008).
15. M. Speidel, A. Jonás, and E.-L. Florin, "Three-dimensional tracking of fluorescent nanoparticles with subnanometer precision by use of off-focus imaging," Opt. Lett. **28**(2), 69–71 (2003).
16. M. F. Juette, T. J. Gould, M. D. Lessard, M. J. Mlodzianoski, B. S. Nagpure, B. T. Bennett, S. T. Hess, and J. Bewersdorf, "Three-dimensional sub-100 nm resolution fluorescence microscopy of thick samples," Nat. Methods **5**(6), 527–529 (2008).
17. M. Badieirostami, M. D. Lew, M. A. Thompson, and W. E. Moerner, "Three-dimensional localization precision of the double-helix point spread function versus astigmatism and biplane," Appl. Phys. Lett. **97**(16), 161103 (2010).
18. G. Grover, S. R. P. Pavani, and R. Piestun, "Performance limits on three-dimensional particle localization in photon-limited microscopy," Opt. Lett. **35**(19), 3306–3308 (2010).
19. S. R. P. Pavani and R. Piestun, "High-efficiency rotating point spread functions," Opt. Express **16**(5), 3484–3489 (2008).
20. S. Quirin, S. R. P. Pavani, and R. Piestun, "Optimal 3D single-molecule localization for superresolution microscopy with aberrations and engineered point spread functions," Proc. Natl. Acad. Sci. U. S. A. **109**(3), 675–679 (2012).
21. S. R. P. Pavani, A. Greengard, and R. Piestun, "Three-dimensional localization with nanometer accuracy using a detector-limited double-helix point spread function system," Appl. Phys. Lett. **95**(2), 021103 (2009).
22. R. T. Borlinghaus, "MRT letter: high speed scanning has the potential to increase fluorescence yield and to reduce photobleaching," Microsc. Res. Tech. **69**(9), 689–692 (2006).
23. G. Donnert, C. Eggeling, and S. W. Hell, "Major signal increase in fluorescence microscopy through dark-state relaxation," Nat. Methods **4**(1), 81–86 (2007).
24. A. Barsic, G. Grover, and R. Piestun, "Sparse reconstructions of overlapping three-dimensional point spread functions using overcomplete dictionaries," arXiv:1308.6826 (2013).
25. I. Heller, G. Sitters, O. D. Broekmans, G. Farge, C. Menges, W. Wende, S. W. Hell, E. J. Peterman, and G. J. Wuite, "STED nanoscopy combined with optical tweezers reveals protein dynamics on densely covered DNA," Nat. Methods **10**(9), 910–916 (2013).
26. C. Maurer, A. Jesacher, S. Bernet, and M. Ritsch-Marte, "What spatial light modulators can do for optical microscopy," Laser Photonics Rev. **5**(1), 81–101 (2011).

1. Introduction

Two types of fluorescence far field optical nanoscopy techniques have been developed thus far. On the one hand, stochastic methods are used in general with photo-switchable molecules. Only a few molecules are activated at the same time, allowing superlocalization of the individual fluorophores [1, 2]. Several frames are recorded and the final image is obtained by combining them. Double Helix (DH) readout [3] with this kind of technique has been implemented for molecular imaging in three dimensions [4]. On the other hand, deterministic methods have been developed where the non-linear response of molecules to excitation is exploited. The more widely used method is Stimulated Emission Depletion (STED) microscopy [5]. The optical apparatus is similar to a scanning confocal microscope, but the excitation beam is surrounded by a so-called depletion beam (or STED beam) which is usually donut shaped and red shifted. This depletion beam quenches, by stimulated emission, all the excited fluorophores around the maximum of the excitation beam. As the stimulated emission process is non-linear, the combination of the two beams results in an effective point spread function (PSF) smaller than the diffraction limited Airy pattern.

Hence, with the most widely used STED arrangement, i.e. a donut profile depletion beam and sufficiently high STED laser intensity, lateral resolution is typically brought down to 20-80nm with organic dyes [6, 7]. Several implementations have been demonstrated to achieve not only a strong improvement in lateral, but also in axial dimension. The most common approach is a circular π phase mask that results in a "bottle" shaped PSF with strong side lobes in the axial direction but reduced intensity in the lateral ones, thus compromising the lateral resolution improvement efficiency [8]. Another modification, the use of adaptive optics to modulate the phase of the depletion beam, allows aberration correction and three dimensional imaging in thick and aberrating samples [9]. However, the same limitation for gain in resolution in both the lateral and axial dimensions remains. Otherwise, an important

#198934 - $15.00 USD Received 7 Oct 2013; revised 17 Nov 2013; accepted 22 Nov 2013; published 9 Dec 2013

gain in resolution in all the directions has been achieved by combining two depletion beams, one for axial improvement and the other for the lateral one [10, 11]. A 4π architecture with opposing lenses has also been demonstrated [12]. Alternatively, STED has been combined with total internal reflection which offers strong axial confinement but only on one surface [13].

The DH rotating beam provides a way to localize precisely the longitudinal position of a source of light. Indeed, the phase of the collected light in a fluorescence microscope can be modulated so that the point spread function is engineered to have a DH shape. As a consequence, the transverse image of a single emitter is made of two lobes and the angle of the line connecting them with respect to the horizontal direction is related to the axial position of the emitter. This angular information can thus be used to extract the axial location of the emitters with high precision. With sufficient fluorescence intensity, axial localization down to 20nm was achieved [4]. Different techniques, such as astigmatism [14], defocusing [15], or bi-plane detection [16], have also been demonstrated in stochastic nanoscopy methods for axial localization.

In this paper, we use the DH method to demonstrate 25nm axial localization of superresolved emitters, with a uniform accuracy over an extended depth of field compared with other localization methods [4, 17]. Since STED decreases the total fluorescence signal and DH is a robust technique for low photon count applications, the combination of the two methods works well [18]. Finally, since DH is an engineered PSF it can be optimized for different systems. The system we demonstrate gives nanometric information in all three directions, with relative simplicity but it is not equivalent to a 3D superresolution system [10, 11]. The only difference between 3D superresolution and axial enhanced localization combined with 2D transversal superresolution is that the later cannot distinguish two laterally colocalized emitters spaced closer in z than the conventional depth of focus. This drawback of the DH-STED approach is compensated by the simplicity and accuracy of the technique compared to a system that has a 3D superresolution PSF such as STED with a "bottle beam" shape focus [8, 10, 11]. The optical system we use for the experimental demonstration of combined DH and STED can also produce programmable wide field phase contrast images. This dual modality is also experimentally demonstrated at the end of the paper.

2. Experimental setup

As illustrated in Fig. 1, a Ti-Sapphire mode locked femtosecond laser pumps an optical parametric oscillator (OPO). A fraction of the pump beam is allowed to go through the OPO without entering the crystal cavity and is used directly for depletion. Pulses are stretched up to about 70ps with a pair of gratings and the phase singularity is generated with a 2π helical phase mask. The OPO output is tuned to 1.266μm and the frequency is doubled with a BBO crystal. The resulting 633nm beam is used for excitation. The two beams are combined with a dichroic mirror and pulses are temporally aligned with a delay line. They are focused with a 1.4 numerical aperture oil immersion objective. The sample is scanned with a piezoelectric stage. The fluorescence is collected with the same objective and imaged with a 200mm tube lens (resulting in a 111X magnification). Two different imaging modes can then be selected with a flip mirror. On one arm, a 60μm pinhole (corresponding to 0.9 airy units) is placed on the imaging plane and light is collected with an avalanche photodiode to realize confocal scanning. On the other arm, a 4-f imaging system creates a wide field image on a CCD camera with a phase only Spatial Light Modulator (SLM) placed on the Fourier plane of the image plane to modulate the PSF. To maximize the transfer function efficiency, the phase pattern used for DH phase modulation was calculated with an optimization algorithm as described in [19].

#198934 - $15.00 USD Received 7 Oct 2013; revised 17 Nov 2013; accepted 22 Nov 2013; published 9 Dec 2013

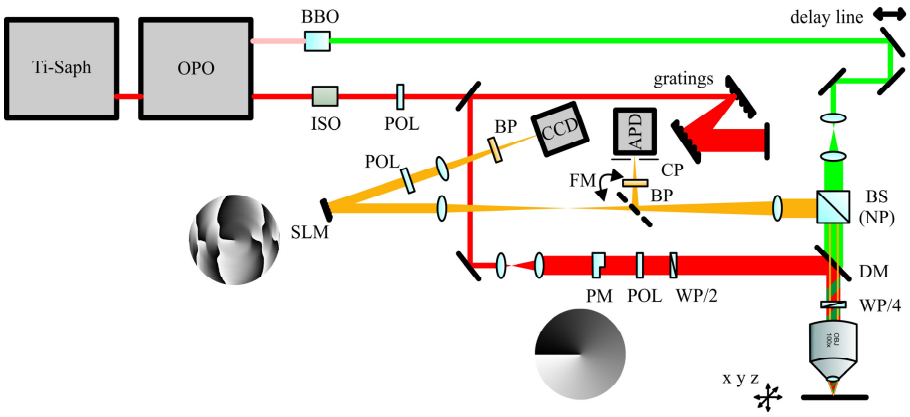

Fig. 1. Schematic of the DH assisted STED setup. OPO-optical parametric oscillator; BBO-barium borate doubling crystal; ISO-Faraday isolator; POL-polarizer; SLM-spatial light modulator; BP-band pass fluorescence filter; WP/2-half wave plate; PM-helical phase mask; BS(NP)-non polarizing beam splitter; DM-dichroic mirror; WP/4-quarter wave plate; CP-confocal pinhole; APD-avalanche photodiode; FM-flip mirror. Inserted pictures show the double helix and donut phase fronts assigned respectively by the SLM and the phase plate, scaled from 0 (white) to 2π (black). Two outputs of a femtosecond OPO system are used for STED microscopy (633nm excitation and 770nm depletion). Two imaging paths are available and can be selected with the flip mirror: one classical confocal scanning microscope optical apparatus with an APD and one path with a SLM followed with a CCD allows phase modulation and DH readout.

3. Method

The beam alignment was accomplished coarsely through recording fluorescence signals and then fine-tuned with light backscattered from nanoparticles. The initial positioning was done by recording the fluorescence signal from an Atto647N dye solution. The confocal pinhole was aligned with the excitation beam by maximizing the detected fluorescence. The spatial and temporal alignment of the two beams was accomplished first by removing the helical phase mask of the depletion beam and overlapping the two Gaussian foci. This superposition was controlled via depletion efficiency measurement out of the fluorescent solution. Indeed, when the two beams overlap the depletion is maximized and consequently the fluorescence minimized. Fine alignment was performed using the backscattered light from single nanometric gold particles. 80 nm particles immobilized on a glass slide were scanned through the foci and the cross sections of the beams were measured as shown in Fig. 2(a). The confocal and depletion PSFs are recorded successively and the donut minimum is aligned to overlap the Gaussian maximum. Sectioning is provided by the confocal pinhole. As illustrated in red in Fig. 2, the longitudinal PSF full width half maximum (FWHM) was measured to be 730nm

The acquisition of three dimensional superresolved images is a two step procedure. The sample is placed on the focal plane of the objective. It is first scanned and a standard STED image is recorded, resolving details below the diffraction limit laterally. As a second step, the focused illumination is brought onto the spots of interest (where some fluorescent molecules are detected) and a DH image is recorded on the CCD, which is then processed to obtain the axial localization of the excited spot. During this second step the STED beam remains on in order to maintain sub-diffraction confinement of the excited area. The final image is then reconstructed with the collected lateral and axial information.

#198934 - $15.00 USD Received 7 Oct 2013; revised 17 Nov 2013; accepted 22 Nov 2013; published 9 Dec 2013

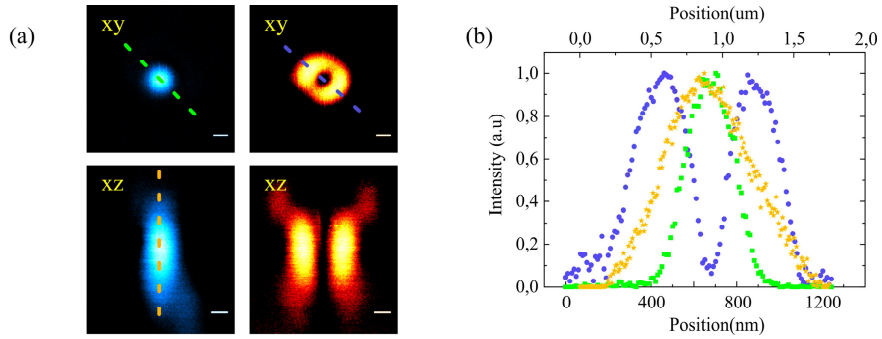

Fig. 2. (a) Point spread functions of the microscope recorded with backscattered light from 80nm gold particles. Scale bars are 200nm. Blue and orange color maps are used respectively for excitation and depletion cross sections. (b) Intensity profiles along the dashed color lines on (a). Bottom axis refers to the lateral profile of the excitation and depletion PSFs that are plotted in green and blue respectively. Top axis refers to the axial cross section which is plotted in yellow. Precise alignment and minimal aberration of the PSFs are critical to observe resolution enhancement with STED. The alignment and the quality of the two beams are controlled by scanning gold particles in the focal plane. Confocal FWHM is measured to be 250nm laterally and 730nm axially.

4. Performance

The lateral resolution of the STED setup was evaluated by imaging 20nm fluorescent beads (crimson, 625/645). As shown in Fig. 3, the FWHM of a single bead profile is measured to be 89nm. By averaging over 20 different beads the FWHM was estimated to be 97nm. The image of the bead is given by the convolution of the excitation PSF with the bead object function. Since the bead has a finite size, the measured value is an upper bound for the effective resolution. Thus, by roughly approximating the bead and the PSF by Gaussians, the actual resolution is evaluated to be 95nm [6]. As illustrated in Fig. 2, the FWHM of the confocal PSF is measured to be 250nm, so the resolution is improved by about 2.5 times with STED. The limited gain in lateral resolution is mainly a result of the limited depletion power available. Indeed, as described above, the initial laser source is split in two beams: one is kept at the initial wavelength for depletion and the other is used to generate the excitation. The OPO system has a fixed power ratio between the two lines and only 20% of the initial laser power can be used for depletion, however, the observed resolution is consistent with the measured saturation intensity obtained on Atto647N solution (characterization data not shown here).

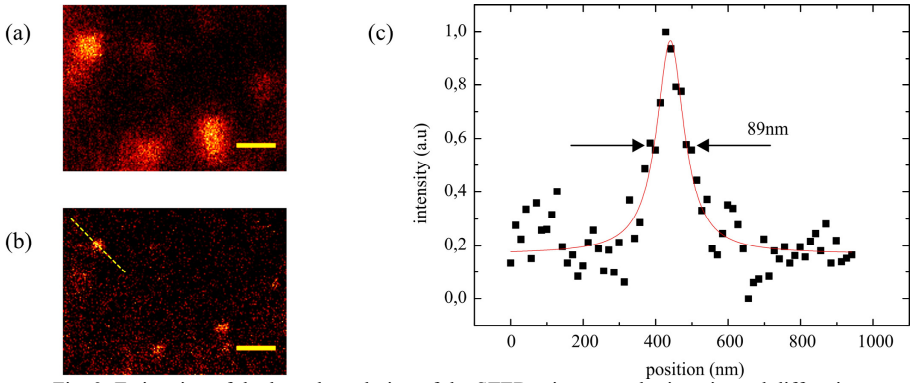

Fig. 3. Estimation of the lateral resolution of the STED microscope by imaging subdiffraction fluorescent emitters. Transverse images of 20nm beads in glycerol immobilized on a glass slide, with confocal (a) and STED (b) microscope. Scale bars are 500 nm. (c) Bead intensity profile along the yellow dashed line on image (b), fitted with Lorentzian function (red line). The measured FWHM for this bead is 89nm. By averaging over a population of beads, the STED microscope resolution is estimated to be 95nm.

#198934 - $15.00 USD Received 7 Oct 2013; revised 17 Nov 2013; accepted 22 Nov 2013; published 9 Dec 2013

Axial localization is calibrated by recording wide field images of a single fluorescent bead at different depths. As illustrated in Fig. 4, the rotation angle of the lobes is recorded for each depth position. This calibration curve allows localization over a large depth of field up to 2μm. The measurement precision depends on the localization repeatability from the lobes, which is dependent on the signal to noise ratio (SNR) [20]. During the acquisition, the presence of the depletion beam in addition to the excitation lowers the photon budget and therefore the precision of the z-localization. Consequently, to evaluate the accuracy of the axial localization in our system, immobilized single beads are illuminated with focused excitation and depletion beams, and the z-localization measurement is repeated several times. This accuracy measurement is represented with the error bars on the calibration curve. The standard deviation of the rotational angle was measured to vary between 0.9 and 1.9° corresponding to a precision between 9 and 22nm, depending on the chosen position. Equivalently, the axial localization precision for single image measurement is below 25nm. This is not the fundamental limit for single image DHPSF detection and it could be potentially improved by the use of a more complex localization estimator [20]. With typical noise conditions, the theoretical limit of the localization accuracy has been shown to be below 1nm [21].

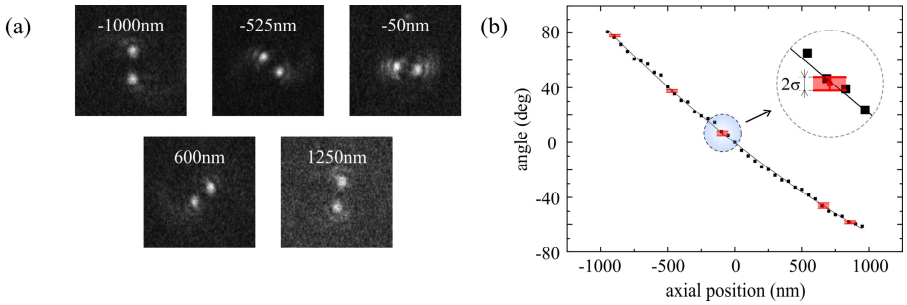

Fig. 4. Axial localization calibration with DH. (a) Images of a fluorescent bead at different axial positions. (b) Corresponding calibration curve of the inclination of the lobes with respect to the bead axial position. Error bars represent the ± standard deviation of the measured angle over 100 images of fixed beads. (For better visualization of those small intervals error bars are represented by lines filled with 2σ height red transparent rectangles centered on the average position. On the upper right hand corner, the area around the third error bar is magnified). To obtain the calibration curve, a single bead image is recorded at every axial position, and the lobes rotational angle is determined on each image. The accuracy of the measurement is evaluated by repeating several times the same localization event with the depletion beam on and calculating the standard deviation.

5. Results

5.1. Imaging beads closer than the diffraction limit

To demonstrate the feasibility of the method, we imaged 100nm diameter fluorescent beads. To obtain a three dimensional sample, beads are embedded in PDMS and spin-coated on a glass slide. Figure 5 shows a group of nanospheres imaged by the confocal microscope, with a resolution of 250nm in Fig. 5(a) and resolved in Fig. 5(b) with DH assisted STED. Figure 5(c) indicates the lateral position of each bead on the STED resolved image where beams are focused for DH readout as shown in Fig. 5(d). This position is determined by centroid localization onto each spot after deconvolution with the Richardson-Lucy Matlab function with a 95nm FWHM Lorentzian PSF for better bead discrimination. Thanks to the superior DH precision, the sample map is reconstructed with the bead positions in three dimensions in Fig. 5(e). For instance, adjacent beads “I” and “II” are resolved. They are measured to be separated by 100nm, 90nm, and 110nm, respectively in the x, y, and z directions. Thus, these two beads with a total separation distance of 173nm are resolved and localized within the

#198934 - $15.00 USD Received 7 Oct 2013; revised 17 Nov 2013; accepted 22 Nov 2013; published 9 Dec 2013

accuracy range defined above in a field of view of 3µm by 3µm. Without the DH localization, the beads would have appeared to be in the same axial plane.

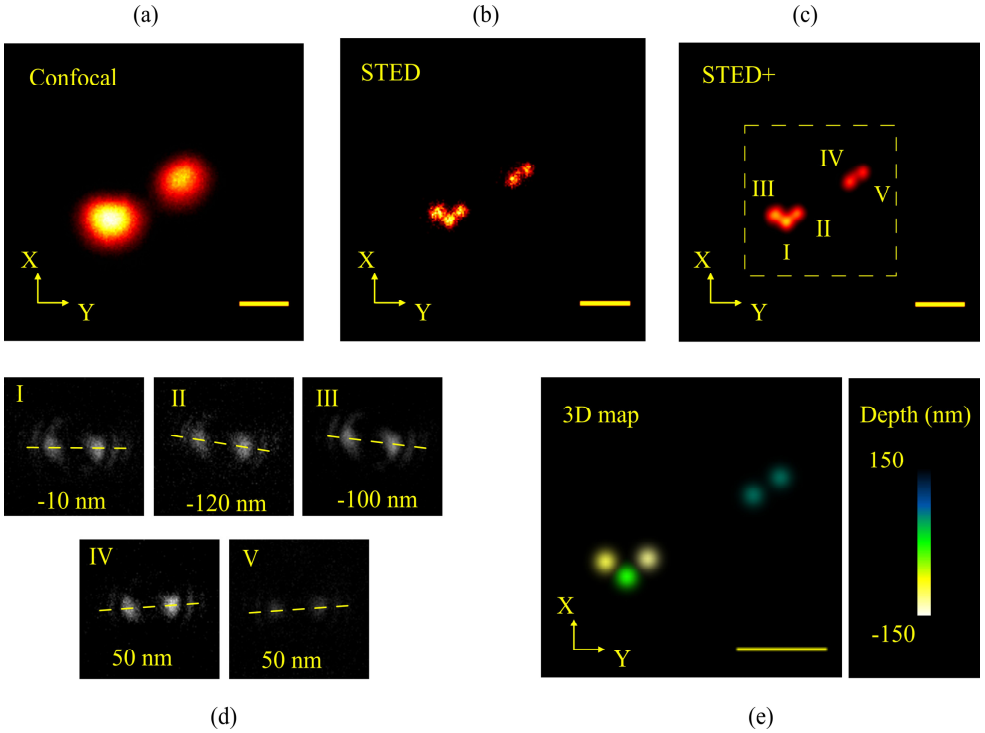

Fig. 5. Three dimensional imaging of a group of 100nm beads immobilized in a PDMS matrix. (a) confocal image (b) corresponding STED image reveals five individual beads (c) Deconvolved STED with numbered cursors on the bead locations and (d) corresponding DH images recorded at these points. (e) 3D representation of the beads position into the dashed boxed delimited on (c) within the focal plane. Scale bars are 500nm. Successive use of STED resolution and DH localization, reveal the three dimensional position of each bead. Although, they appear as a large cluster merged in the focal plane on the confocal image.

5.2. Reducing photobleaching

The gain in the resolution with stimulated emission requires a high depletion intensity to obtain an efficient confinement of the excitation volume. Consequently, photobleaching is the main drawback of STED microscopy. With this method, during each depth localization acquisition the beams are immobilized on the sample. This fixed exposure with both beams results in severe degradation of the signal as shown in Fig. 6(a). The main solution for reducing photobleaching consists of decreasing the amount of time the fluorophores are continuously excited, either by accelerating the scan speed [22] or by reducing the laser repetition rate [23]. Thus, to reduce photobleaching during depth readout, we chop the two beams at 10 kHz. As illustrated in Fig. 6(b), this improves the life time of the fluorescence beads. Exponential decay fitting, results in decay time of 22.8s with both beam illumination, 36.3s with chopping, and more than 5 min without depletion beam. Thus, chopping gives equivalently 1.2 times more photons for the first 10 seconds from a single bead and improves DH axial localization.

#198934 - $15.00 USD Received 7 Oct 2013; revised 17 Nov 2013; accepted 22 Nov 2013; published 9 Dec 2013

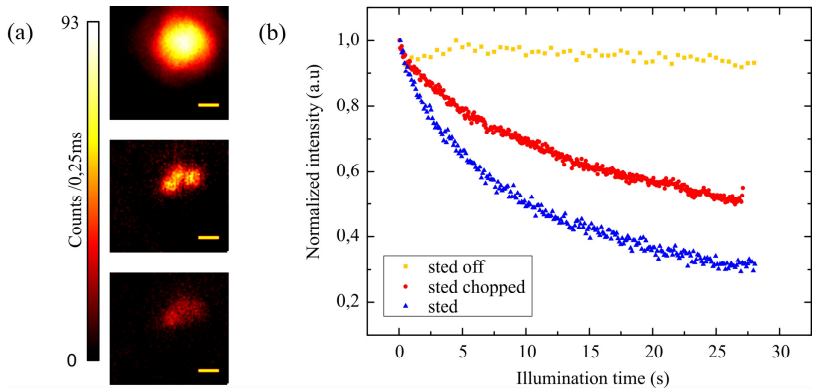

Fig. 6. Photobleaching induced by STED beam. (a) Images of three fluorescent beads represented with the same intensity scaling. From top to bottom: initial confocal scan, consecutive STED image before and after DH localization (around 2s illumination on each bead). (b) Fluorescence photoresistance of 100nm beads under focused light excitation and depletion beam off (yellow), on (blue) and both beams chopped (red). Each curve on (b) is averaged out of 10 single beads. The three scanning images show STED beam induces strong photobleaching during prolonged excitation for the DH axial localization. Fluorescent bead photoresistance can be improved by 20% by chopping the beams.

6. Discussion

As demonstrated above, DH assisted STED allows the discrimination of fluorescent emitters spaced closer than the diffraction limit and the precise localization of individual emitters in the axial dimension. However, the technique relies on the fact that, STED lateral confinement and confocal sectioning are sufficient to isolate every single emitter. In other words, if the sample is so highly concentrated such that two separate fluorescence sources strictly overlap transversely and are closer than confocal axial resolution in depth, they cannot be directly resolved. However, recent work has demonstrated progress towards resolving overlapping PSFs through further data post-processing via a PSF fitting algorithm [24]. Additional work addressing this limitation to resolve a cluster of overlapping emitters with a high three dimensional localization precision is ongoing.

However, if the emitters are resolved by lateral superresolution, the combination of STED imaging with DH axial localization presents advantages. Indeed, DH-STED enables depth localization of a superresolved object with high, uniform precision through an extended depth of field, thereby providing axial information with a single lateral scan which is otherwise not possible with three dimensional STED imaging.

Moreover, the importance of wide field imaging and a phase contrast mode in addition to STED, for overall context understanding of transparent samples, has been recently highlighted [20]. Furthermore, the helical phase mask has been used both for STED beam generation and spiral phase contrast imaging [20]. As demonstrated in the appendix section in Fig. 7, the placement of the SLM can allow for dynamically switching to phase contrast wide field imaging before scanning the region of interest. As STED imaging is entirely dependent on the fluorescent staining, the ability to reveal surrounding non-stained structures should facilitate the use of DH-STED method with biological sample.

The major advantage of STED over stochastic methods is the acquisition time. In STED microscopy, fast scanning mechanisms lead to several frames per second acquisition within a reasonable field of view [21]. In our method, the full 3D scanning image cannot be recorded point by point entirely with the CCD because of the sensor speed and induced photobleaching. These limitations however are not fundamental. Indeed, the DH reduces the collection efficiency and a 100ms exposure time is required to collect enough light to image the DH lobes. As detailed above in Fig. 6, chopping limits photobleaching induced by the prolonged illumination with the two beams. However, as for conventional STED imaging

#198934 - $15.00 USD Received 7 Oct 2013; revised 17 Nov 2013; accepted 22 Nov 2013; published 9 Dec 2013

photobleaching remains the main limitation. Figure 6 indicates that multiple DH assisted STED scans with our optical arrangement would be challenging. However, our initial demonstrations have shown the feasibility of the method to localize within a single plane. Moreover, the use of a sensitive multiple point detector, like an APD array, as a single sensor would allow a decrease in the time the laser beams dwell on a single emitter by several orders of magnitude (typical dwell time for STED is 10us-1ms compared with 100ms camera exposure). This could dramatically decrease acquisition time and improve fluorescence degradation by photobleaching and allow fast multiple slice 3D imaging with STED [11], while benefitting from the increased DH axial localization precision.

7. Conclusion

We demonstrated the first realization of STED microscopy assisted with DH axial localization. We quantified the performance of the system by imaging single immobilized beads on a surface. Following this, we superresolved an assembly of subdiffraction beads which were axially located within a single confocal imaging plane and localized those in depth with 25 nm precision. The method combines the advantages of STED and DH localization, a large depth of field, fast acquisition time, and nanometric accuracy in three dimensions. The potential long term significance of this work lies in the fact it combines two methods for which there is a reasonable expectation that future improvement on the emitter brightness and the detector sensitivity can lead to increased performance. We expect that this technique can find use in applications requiring dynamic three dimensional far field imaging with high precision, such as protein tracking along immobilized DNA [25] or topographic measurements of cellular structures.

Appendix: Wide field phase contrast imaging

An interesting feature of our experimental apparatus is the possibility to use it to obtain phase contrast imaging. Indeed, thanks to the phase only SLM in the imaging path, any type of Fourier filtering can be envisaged [26].

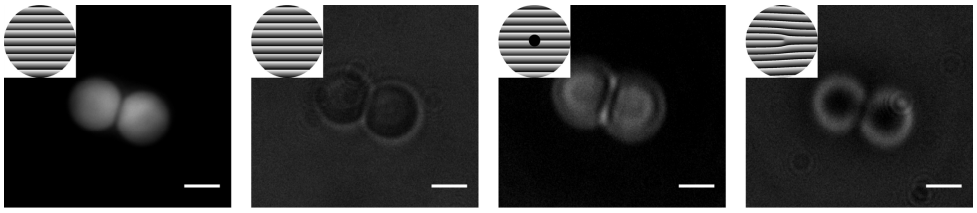

(a) (b) (c) (d)

Fig. 7. Images of two 1.5µm fluorescent beads immobilized on a glass slide. (a) Wide field fluorescence image. (b) White light illumination image. (c) and (d) Examples of filtering in the Fourier domain: dark field (c) and spiral contrast (d). Insets on the left hand corners represent corresponding phase pattern projected onto the SLM. Scale bars are 1µm.

Figure 7 illustrates two different well known phase contrast techniques demonstrated with 1.5µm fluorescent beads. The fluorescence image in Fig. 7(a), on which DH assisted STED could reveal subdiffraction details, can be associated with complementary information from the phase contrast techniques. The dark field image in Fig. 7(c), obtained by blocking the zeroth-order Fourier component reveals non fluorescent structures that are badly contrasted on wide field imaging as shown in Fig. 7(b). Finally, the spiral phase contrast image, obtained with a helical phase pattern, enhances the edges in Fig. 7(d).

Acknowledgments

We would like to thank Prof. Bart Deplancke for helpful discussions and Dr. Marcel Leutenegger for his advices about the STED microscope implementation. We thankfully acknowledge support from Swiss SystemX.ch through grant N°2010/072.